Path Planning in Unstructured Urban Environments for Self-driving Cars

Anderson Mozart, Gabriel Moraes, Rânik Guidolini, Vinicius B. Cardoso, Thiago Oliveira-Santos, Alberto F. De Souza[*] and Claudine Badue
Departamento de Informática, Universidade Federal do Espírito Santo, Vitória, Brazil

Keywords: Path Planning, Unstructured Urban Environments, Self-driving Cars, A* Algorithm.

Abstract: We present a path planner for unstructured urban environments (PPUE) for self-driving cars. PPUE receives initial and goal poses as input, as well as maps of the environment. It employs a hybrid A* algorithm with two heuristics for generating paths, which are smoothed using Conjugate Gradient optimization. Different from previous works, PPUE uses: (i) an obstacle distance grid-map, instead of an occupancy grid-map, for representing the environment; and (ii) an accurate but simple collision model of the car. We have examined PPUE's performance experimentally in simulated and real world scenarios. Our results show that PPUE computes smooth and safe paths, which follow the kinematic constraints of the vehicle, fast enough for suitable real world operation.

1 INTRODUCTION

The path planning task of self-driving cars can be formulated as the problem of finding a sequence of poses, $P = \{p_1, p_2, \dots, p_i, \dots, p_{|P|}\}$, from the current car pose, p_1, to a desired pose, $p_{|P|}$, where each pose is a position in the world, defined as a 2-D coordinate pair, the self-driving car's orientation at this position, and the direction of movement (forward or reverse), i.e., $p_i = (x_i, y_i, \theta_i, r_i)$. Depending on the operating scenario, path planning can be more or less complex. Urban self-driving cars typically have two main operating scenarios: road driving and parking. In road driving, path planning is typically simpler thanks to the road-network structure. To improve safety, roads have vertical and horizontal signalizations that simplify driving, and, therefore, path planning on them. Path planning on parking lots and other non-structured areas cannot benefit much of vertical and horizontal signalization, which makes path planning in such scenarios more complex.

We have developed a self-driving car, named Intelligent Autonomous Robotic Automobile (IARA, Figure 1), whose autonomy system follows the typical architecture of self-driving cars (Badue et al., 2020). Our self-driving car is based on a Ford Escape Hybrid tailored with a variety of sensors and processing units. Its autonomy system is composed of many modules, which include a localizer (Veronese et al., 2016), a mapper (Mutz et al., 2016), a moving obstacle tracker (Sarcinelli et al., 2019), a traffic signalization detector (Possatti et al., 2019; Torres et al., 2019), a route planner, a path planner for structured urban areas, a behavior selector, a motion planner (Cardoso et al., 2017), an obstacle avoider (Guidolini et al., 2016), and a controller (Guidolini et al., 2017), among other modules.

In this paper, we propose a path planner for unstructured urban environments (PPUE) for our or any other self-driving car. The proposed path planner for unstructured urban environments (for now on, path planner for short) is similar to that presented by Dolgov et al. (2010) – one of the most preeminent path planners in the literature based on the A* algorithm – but improve on it in several aspects. The contributions of this paper are these improvements, which can be summarized as: (i) the use of an obstacle distance grid-map instead of an occupancy grid-map (Thrun, Burgard & Fox, 2006) to represent the environment; and (ii) a more accurate but simple collision model of the car, which

[*] Senior Member, IEEE

Mozart, A., Moraes, G., Guidolini, R., Cardoso, V., Oliveira-Santos, T., F. De Souza, A. and Badue, C.
Path Planning in Unstructured Urban Environments for Self-driving Cars.
DOI: 10.5220/0010559602900300
In *Proceedings of the 18th International Conference on Informatics in Control, Automation and Robotics (ICINCO 2021)*, pages 290-300
ISBN: 978-989-758-522-7

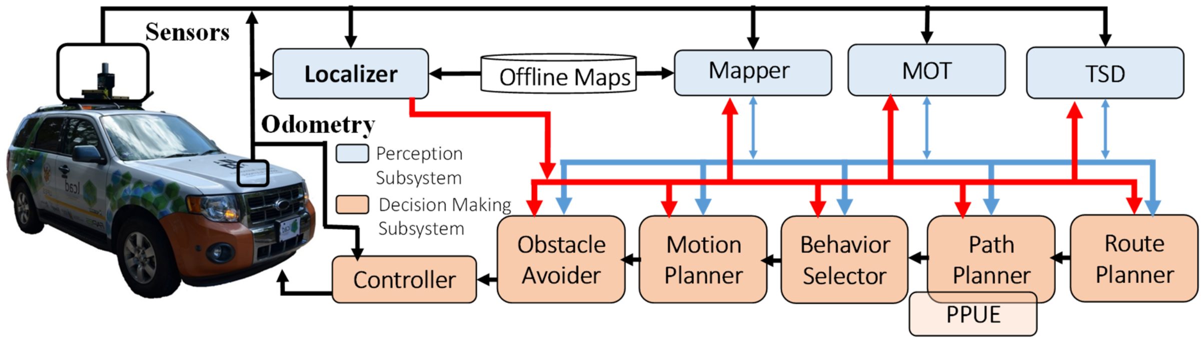

Figure 1: Intelligent Autonomous Robotic Automobile (IARA) and its autonomy software system. In light blue, perception modules. In orange, decision making modules. TSD denotes Traffic Signalization Detection and MOT, Moving Objects Tracking. Red arrows show the State of the car, produced by its Localizer module and shared with most modules; blue arrows show the car's internal representation of the environment, jointly produced by several perception modules and shared with most decision making modules. See details in Badue et al. (2020).

simplifies the implementation of the path planner algorithm. To evaluate the performance of the proposed path planner, we employed our self-driving car simulator and different scenarios where the car had to make different maneuvers to achieve the goal. We measured the hybrid A* search running time, the full running time (which includes path smoothing step), the number of nodes expanded by the hybrid A* search, and the length of the final smoothed path. To assess the benefits of the use of the obstacle distance grid-map and the collision model of the car, we also measured the running time to create the map and to query it for the distance from the car to the nearest obstacle. Finally, we conducted real-world experiments using our self-driving car in a parking lot to examine the real world performance of the solution. Experimental results have shown that our planner allows our self-driving car to find a proper path in an unstructured environment in reasonable time, with running times from 0.42 s to 0.61 s for a path of about 70 m.

2 RELATED WORKS

Several techniques have been proposed in the literature for implementing path planners for non-structured urban environments. Relevant path planner implementations include graph search based planners (Dolgov et al., 2010; Chu et al., 2015; Yoon et al., 2015; Urmson et al., 2008; Wang, 2019) sample based planners (Ghosh et al., 2019), and deep neural network based planners (Kicki, Gawron & Skrzypczyński, 2020; Moraes et al., 2020). Among those based on graph search, Dolgov et al. (2010) presented a path planner based on the hybrid A* algorithm for the autonomous car Junior, that finished second in the 2007 DARPA Urban Challenge (Montemerlo et al., 2018). Our path planner is similar to that of Dolgov et al. (2010), but refines it in two main aspects: the use of an obstacle distance grid-map (instead of an occupancy grid-map) and of a more precise collision model of the car, which allowed computing the distance from the car to the nearest obstacle accurately and quickly.

Other authors propose other variants of the A* algorithm for path planning. Urmson et al. (2008) proposed the anytime D* to compute a path for the self-driving car Boss (Carnegie Mellon University's car that claimed first place in the 2007 DARPA Urban Challenge). Both anytime D* and hybrid-state A* algorithms merge two heuristics – one non-holonomic, which disregards obstacles, and the other holonomic, which considers obstacles – and were used for path planning in an unstructured environment (parking lot). Chu et al. (2015) proposed a variation of A* to build a path that considers car's kinematic constraints, which ignores the resolution of grid cells and creates a smooth path. Yoon et al. (2015) proposed a variation of A* to compute a path that accounts for kinematic constraints of the autonomous vehicle Kaist. None of these works use obstacle-distance maps.

Wang (2019) proposes a variant of the Hybrid A* (i-AGT) that conducts selective expansion for a node, where only the control actions with the highest priority are applied, and a bidirectional A-search (BAGT), where two trees are constructed simultaneously from the initial and goal state. The path planner was tested in a simulation of a car in a parking lot, and its computation time, complexity of the tree and path length were measured. Experimental results indicate that i-AGT and BAGT are significantly faster than the normal Hybrid A*, but in some cases, the BAGT is prone to fail (Wang, 2019).

Among those based on sampling, Ghosh et al. (2019) propose a kinematically constrained Bi-RRT (KB-RRT) algorithm, where the expansion of RRT is restricted to feasible regions of the state space, which avoids unnecessary growth of the RRT. In this approach, two RRTs are created from the initial and goal state, and are grown until they become connected, when a solution is found. This solution does not guarantee an optimal trajectory, however.

Among those techniques based on neural networks, Kicki, Gawron and Skrzypczyński (2020) presented a path planner that employs a gradient based self-supervised learning algorithm to predict feasible paths. The neural network receives a representation of the environment, the initial and desired final robot poses, and generates a path spline defined as a 5-th degree polynomial. They evaluated the performance of their path planner in simulation experiments, in which overtaking maneuvers, perpendicular parking and oblique parking were considered. Their experimental results showed that their path planner can be 14 times faster than other comparing planners and serve as a generator of the initial solutions for other complete path planning algorithms. Moraes et al. (2020) presented an image-based path planner for self-driving cars, which receives a front-face camera image and the current car pose, infers a cubic spline path model, generates the path in the car coordinate system and transforms its poses to the world coordinate system. They examined the performance of their path planner in real world scenarios. Their experimental results showed that the path planner is capable to generate paths on straight and curved sections of the lane, but might fail on forks in the road. Path planner based on neural networks does not guarantee optimality nor completeness, however.

3 A PATH PLANNER FOR UNSTRUCTURED ENVIRONMENTS

The hybrid-state A* algorithm of PPUE receives as input the Initial Pose, p_1, the Final Pose, $p_{|P|}$, an Obstacle Distance Grid-Map ($\mathbf{ODGM}$), a Goal Distance Map ($\mathbf{GDM}$), and a Nonholonomic Heuristic Cost Map ($\mathbf{NHCM}$). Each cell of the $\mathbf{ODGM}$ holds the distance from itself to the nearest obstacle – the way we compute this map online and the benefits of using it are described in Section 3.2. Each cell of $\mathbf{GDM}$ holds the length (travelled distance) of a holonomic path from itself to the goal considering obstacles – see Section 3.4. Finally, each cell of $\mathbf{NHCM}$ holds the length of a nonholonomic path from itself to the goal without considering obstacles – the cost of computing this map is high, but we can compute it only once and offline, as detailed in Section 3.5. The output of the hybrid-state A* algorithm is an optimal path $P' = \{p_1, p_2, \dots, p_i, \dots, p_{|P|}\}$, which may not be suitably smooth for an Ackermann steering robot. Therefore, we smooth this path producing the path P , as described in Section 3.8. The smoothed path is sent to the Behavior Selector module for execution (see Figure 1). Our implementation of the hybrid-state A* algorithm is presented in Algorithm 1 and detailed below.

Algorithm 1: Hybrid-State A* Algorithm.

```
Input: $p_1, p_{|P|}$, $\mathbf{ODGM}$, $\mathbf{GDM}$, $\mathbf{NHCM}$
Output: $P$
1:  $n_1 \leftarrow (p_1, 0, 0, \text{NULL})$
2:  $\mathbf{GSM}$[.]← (Not visited, 0)
3:  $FH \leftarrow \{n_1\}$
4:  $\mathbf{GSM}[n_1.p] \leftarrow$ (Open, $g(n_1)$)
5:  while $FH \neq \emptyset$ do
6:    $n \leftarrow FH.pop()$ // get node $n$ with minimum $n.f$ from $FH$
7:    if $\mathbf{GSM}[n.p].s \neq$ Closed then
8:      $\mathbf{GSM}[n.p].close()$
9:      if $is\_goal(n.p, p_{|P|})$ then
10:       $P' = get\_path(n)$
11:       return $P'$
12:     else
13:       $N \leftarrow \{expand\_node(n, \mathbf{ODGM})\}$
14:       for $n' \in N$ do
15:         $n'.g \leftarrow g(n')$
16:         $n'.f \leftarrow f(n')$
17:         $n'.parent \leftarrow n$
18:         if $\mathbf{GSM}[n'.p].s \neq$ Closed and
19:           ($\mathbf{GSM}[n'.p].s$ = Not visited or
20:             ($\mathbf{GSM}[n'.p].s$ = Open and $\mathbf{GSM}[n'.p].g > n'.g$)) then
21:           $\mathbf{GSM}[n'.p]$ = (Open, $n'.g$)
22:           $FH \leftarrow FH \cup \{n'\}$
23: return $\{\emptyset\}$ // path not found
```

3.1 Hybrid A* Search

Different from the standard A*, where the search is performed in a graph, in the hybrid-state A* algorithm the search is performed in a Grid State Map ($\mathbf{GSM}$). Algorithm 1 finds P' using the $\mathbf{GSM}$ and a Fibonacci Heap, FH, of nodes. $\mathbf{GSM}$ is a 4D grid-map indexed by discretized poses, $p_i = (x_i, y_i, \theta_i, r_i)$, where each cell holds a state and a value. The state can be "Not visited", "Open", or "Closed", while the value is computed by a path-cost function, $g(.)$. We use the Fibonacci Heap, FH, for efficiently implementing the list of nodes being handled by the algorithm at each instant of time.

Each node, n, holds: a candidate pose of P'; the cost f, computed by the cost function $f(.)$; the cost g, computed by the cost function $g(.)$; and a pointer to its parent node. In the following, we detail these cost functions.

The hybrid A* algorithm is guided by the costs f and g of each node. It tries and finds a path from p_1 to $p_{|P|}$ traversing $\mathbf{GSM}$ through the cells with the smallest f and g, starting with the cell set with p_1. To examine all possible paths allowed by the discretization of the space provided by $\mathbf{GSM}$ is too expensive; hence, the use of a search algorithm such as the hybrid A* is a practical alternative. Starting from an initial node we call n_1, which is set using p_1 (line 1 of Algorithm 1), the algorithm expands new nodes, n', whose poses obey the robot's nonholonomic restrictions and that do not collide with obstacles. The costs f and g of n' are computed by the functions $f(n')$ and $g(n')$, which are given by

$$f(n') = penalties(n') + g(n') + h(n') \quad (1)$$

and

$$g(n') = g(n) + |n.p - n'.p|, \quad (2)$$

where

$$h(n') = \max\left(\mathbf{GDM}[n'.p], \mathbf{NHCM}\left[p_{|P|} - n'.p\right]\right). \quad (3)$$

So, as shown in (1), $f(n')$ is the sum of the costs associated with n'. Let's start by examining the costs associated with n' by the $penalties(n')$ term in (1). $penalties(n')$ are given by

$$\begin{gathered} penalties(n') = \frac{1}{\mathbf{ODGM}[n'.p]} + \\ w_1 \times |n.p - n'.p| \times n'.p.r + \\ w_2 \times [n'.p.r \neq n.p.r], \end{gathered} \quad (4)$$

where w_1 and w_2 are weights.

In (4) and throughout the text, we use the notation $x.y$ to refer to the element y of x ($n'.p$ is the pose element of n'). So, by its first term, $penalties(n')$ grows with the inverse of the distance between the pose of the node n' and the nearest obstacle. By the second term, $penalties(n')$ increases with w_1 times the Euclidean distance between the poses of the nodes n and n' if the direction of movement from n to n' is reverse (i.e., $n'.p.r = 1$). Finally, by the third term, $penalties(n')$ increases with w_2 in case of a change in the direction of movement (i.e., $n'.p.r \neq n.p.r$). The weights w_1 and w_2 are parameters of the algorithm.

The next term of (1) is $g(n')$ itself, which is given by (2). As shown in (2), $g(n')$ is equal to $g(n)$ plus the Euclidean distance between the poses of the nodes n and n'. Finally, the last term of (1) is $h(n')$, which is given by (3). As shown in (3), $h(n')$ is given by the maximum of two terms: $\mathbf{GDM}[n'.p]$ and $\mathbf{NHCM}\left[p_{|P|} - n'.p\right]$. The first term represents the cost of going from $n'.p$ to $p_{|P|}$ following a path that considers obstacles, but not the nonholonomic restrictions of the car. We detail how we build $\mathbf{GDM}$ online in Section 3.4. The second term represents the cost of going from $n'.p$ to $p_{|P|}$ following a path that obeys the nonholonomic restrictions of the car, but that does not consider obstacles. This second term is important for increasing the cost of paths that arrive at the goal with wrong robot orientation. We detail how we build the $\mathbf{NHCM}$ offline and how we use it online to compute this cost in Section 3.5.

Algorithm 1 starts by initializing the initial node, n_1, with the tuple $(p_1, 0, 0, \mathrm{NULL})$, in line 1, the whole $\mathbf{GSM}$ with the tuple (Not visited, 0), in line 2, and FH with a list of nodes containing n_1 only, in line 3. After this initialization and before the main loop, in line 4 the algorithm sets the cell of $\mathbf{GSM}$ where p_1 is mapped to with the tuple (Open, $g(n_1)$). This marks this cell as Open and sets the cost of this cell according to the function $g(.)$.

The main loop of Algorithm 1 starts by testing if FH is empty, in line 5, which will not be the case at start time due to its initialization in line 3. In line 6, the algorithm gets the node n with minimum cost f from FH. The algorithm proceeds by examining if the cell indexed by the pose of the node n is closed, in line 7. If it is not closed, in line 8, the algorithm closes the cell. Then, the algorithm checks, in line 9, if the current node is near enough to the goal using the function *is_goal*(). In this case, it computes the path using *get_path*(), which basically goes back in the sequence of nodes from the current node, n, up to initial node, n_1, using the pointer to the parent node that every node maintains, and returns the path P', in line 11. If *is_goal*() returns false, the algorithm continues from line 12 onwards.

In line 13, the current node taken from FH is expanded producing a set of nodes we call N (the function *expand_node*() is described in Section 3.6). This expansion is the mechanism employed by the algorithm to search for a solution in a space of alternatives where it can move forwards, backwards, left, right, or straight. For the set of possible expansions, the algorithm, starting in line 14, examines each one of the expansion alternatives and computes, for each one of them, represented by n',

$n'.g$, $n'.f$ and the pointer to the parent of n', i.e., n, in lines 15 to 17, respectively.

Once n' is computed, in lines 18 to 20, the algorithm examines if its cell of $\mathbf{GSM}$ is not closed, in line 18, and not visited, in line 19, or if its cell is open and the value g of the cell is larger than the value g of n'. If the conditions examined in lines 18 to 20 hold true, the cell of $\mathbf{GSM}$ pointed by the pose of n' is set as open and the value of the cell of $\mathbf{GSM}$ is set to the value g of the node n', in line 21. Then, this node is added to the Fibonacci heap FH, in line 22. After examining all possible expansions of node n in lines 13 to 22, the algorithm goes back to line 5 and checks if the Fibonacci Heap is empty. If not, it takes the node with the minimum value f from the heap – many of them might have been added in line 22 – and continues the process, trying to find a node that is near enough to the goal as tested in line 9. If one such node is found, the path P' has been found and it is returned by the algorithm in line 11. If no path is found after exploring all possible cells of $\mathbf{GSM}$, the Fibonacci Heap will be found empty in line 5; that is, there will be no more nodes to examine. In this case, the algorithm will terminate in line 23 returning an empty path.

3.2 Obstacle Distance Grid-Map (ODGM)

A contribution of this paper is the use of an $\mathbf{ODGM}$ instead of an occupancy grid-map (Dolgov et al., 2010) to represent the obstacles in the environment. Each cell of $\mathbf{ODGM}$ keeps its distance to the nearest obstacle; so, to find out the distance from a position to the nearest obstacle, we simply query the $\mathbf{ODGM}$ cell where the position is mapped to.

Figure 2 illustrates an $\mathbf{ODGM}$ of the parking lot where we conducted real-world experiments using our self-driving car. In the $\mathbf{ODGM}$ of Figure 2, darker cells represent regions closer to obstacles, while lighter cells indicate areas farther from obstacles. The uniformly lighter cells in the middle of the map represent areas whose distances from obstacles are greater than a threshold and are represented by a constant value. $\mathbf{ODGM}$ is computed online using the current occupancy grid-map of the same area and dynamic programming.

3.3 Collision Model of the Car

Another contribution of this paper is the use of a precise, yet simple collision model of the car to compute the distance from the car to the nearest obstacle in the context of unstructured path planning. The collision model of the car is used to: (i) compute the first term of $penalties(n')$, in (4) (see Section 3.1); (ii) verify if expanded nodes, n', collide with obstacles (Section 3.6); and (iii) check for collisions during path smoothing (Section 3.8).

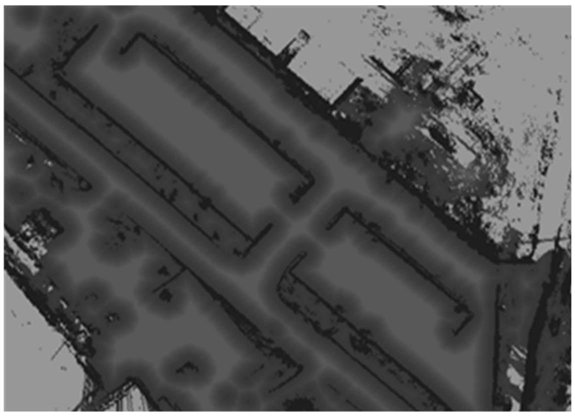

Figure 2: ODGM. Darker cells represent regions closer to obtacles, while lighter cells farther from obstacles.

The car is modeled by a set of 5 equally spaced circles with equal radii, R. To obtain the distance from the car to the nearest obstacle, we verify the obstacle distance held by the $\mathbf{ODGM}$ cells to where the centers of the car model circles mapped, and return the smallest distance. If the returned distance is smaller than R, it is considered as collision. Figure 3 shows the collision model of the car (five circles) with an excerpt from an occupancy grid map in the background.

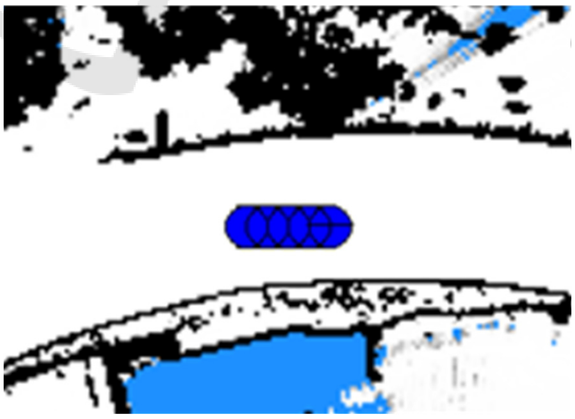

Figure 3: Collision model of the car (five circles) superimposed on a blue rectangle with an excerpt from an occupancy grid map in the background. The blue rectangle indicates the current car's pose. In the occupancy grid map in the background, white cells represent free regions, grey cells represent occupied regions and blue cells represent unknown regions.

3.4 Goal Distance Map (GDM)

Each cell of **GDM** holds the distance from itself to the goal, $p_{|P|}$. To compute a **GDM,** we use the Exact Euclidean Distance Transform (EEDT), proposed by Elizondo-Leal, Parra-González, and Ramírez-Torres (2013) which receives as input a discretized version of the current **ODGM** and $p_{|P|}$. We discretize **ODGM** using a distance threshold (0.5 m) – cells closer to obstacles than this threshold are set to 1, otherwise, zero.

In Figure 4(a), we show an example of **GDM** computed using EEDT, where the goal is the center of the map and there is only a vertical line as obstacle. In Figure 4(b), we show the same example, but using dynamic programming for computing **GDM**. As can be seen in these figures, EEDT provides a more precise map. **GDM**s computed using dynamic programing have the disadvantage of making search algorithms prefer paths that follow the artifacts present in maps produced this way (the lines in form of star irradiating from the goal in Figure 4(b)).

In Figure 4(c), we show the **GDM** of a parking lot used in the experiments. The goal $p_{|P|}$ is represented by a small red circle. As can be seen in the figure, we use a **GDM** with reduced resolution for closing gaps present in **ODGM** that would otherwise allow misguided distances to goal in **GDM**.

3.5 Nonholonomic Heuristic Cost Map (NHCM)

Each cell of **NHCM** holds the nonholonomic distance from $n'.p$ to the **NHCM** center, which represents the goal, $p_{|P|}$. We access a cell in this map using the vector $v(x, y, \theta) = p_{|P|} - n'.p$ (see (3)); so, **NHCM** is a tridimensional map indexed by a discretized version of v. We used Reed-Shepp curves (Reeds & Shepp, 1990) to compute this map. The cost stored in each cell $\mathbf{NHCM}\left[p_{|P|} - n'.p\right]$ is equal to the length of the Reed-Shepp curve that takes the car from a pose $n'.p$ to $p_{|P|}$. The length of this curve (or path) depends heavily on the orientation of the current pose, $n'.p$, and the Final Pose, $p_{|P|}$. In our implementation, **NHCM** does not consider obstacles; so, as Dolgov et al. (2010), we were able to compute it offline and store it as a lookup table.

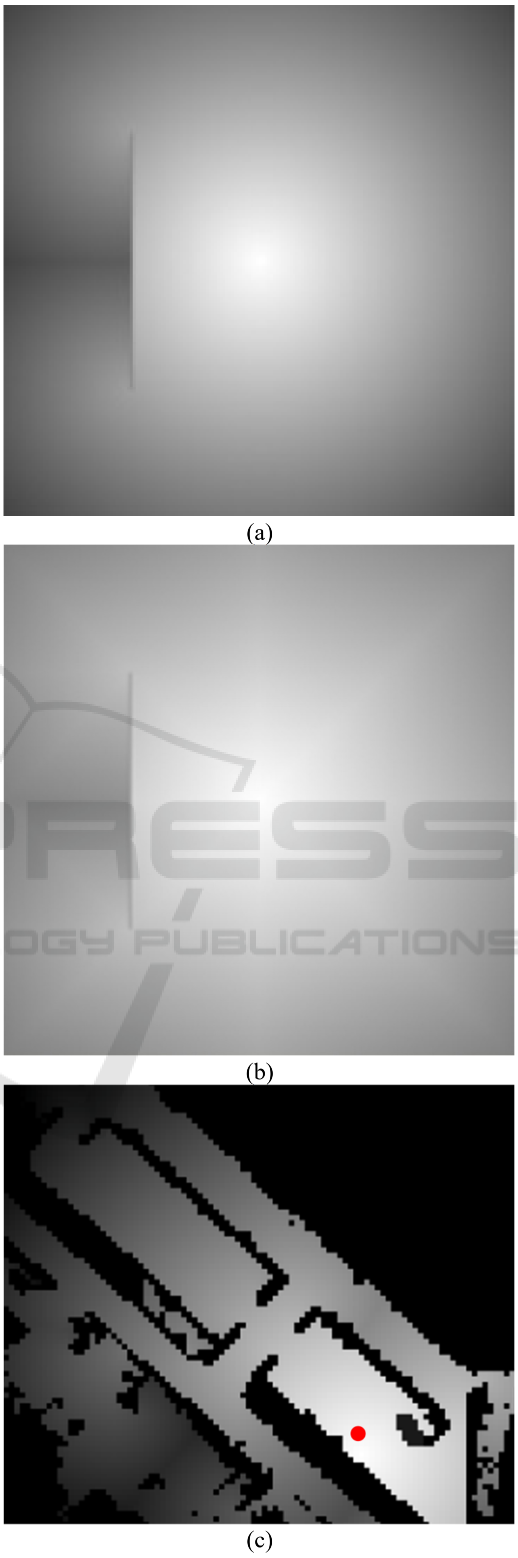

Figure 4: (a) Example of GDM obtained by EEDT. (b) Same example of (a) but computed using dynamic programming. (c) GDM of a parking lot used in experiments.

3.6 Expansion of Nodes

Since we use a nonholonomic robot (a car), the expansion of a node must follow its kinematic constraints. The method *expand_node*() of Algorithm 1 performs node expansion and receives the current node, n, and $\mathbf{ODGM}$ as input. *expand_node*() computes a set, N, composed of up to 6 poses $n'.p$. These poses are computed simulating the car movement from $n.p$ to poses resulting from moving the car forwards and backwards for a fixed distance, d, while steering to max-left, straight, and to max-right. This results in 6 $n'.p$ poses. However, if any of these poses results in a collision in $\mathbf{ODGM}$, it is not include in the set N.

3.7 Goal Proximity Verification and Reed-Shepp Path

The method *is_goal*() verifies if the current node, n, is close enough to the goal and, if it is, the search terminates. If it is not, *is_goal*() computes, for every $k(.)$ nodes examined, where $k(.)$ is a function that returns a value that decreases as $n.p$ gets closer to the Final Pose, $p_{|P|}$, a Reed-Shepp path between $n.p$ and $p_{|P|}$. If the Reed-Shepp-path's poses have no collisions and there is no change of direction of movement in this path, (i) it is appended to the path computed so far from $n_1.p_1$ to $n.p$, (ii) n receives the value of the last node of the Reed-Shepp path, and (iii) *is_goal*() returns true. Otherwise, *is_goal*() returns false. The requirement of no change of direction of movement in the Reed-Shepp path is enforced for avoiding paths with too many changes of direction near the goal.

3.8 Path Smoothing

The paths produced by Algorithm 1 are composed uniquely by segments of a fixed distance, d, forwards and backwards, while steering to max-left, straight, and max-right. To improve passenger comfort and safety, we smooth this path using the Conjugate Gradient (CG) optimization algorithm. We employ CG for minimizing the following objective function:

$$C(P') = \sum_{i=1}^{|P'|} c_s^i + c_o^i + c_c^i. \quad (5)$$

$C(P')$ is equal the sum of three costs: the smoothness cost, c_s^i, and the obstacle cost, c_o^i, and the curvature cost, c_c^i. For minimizing $C(P')$, CG moves the poses p_i of P', using the gradient of $C(P')$ as a guide. Actually, P' is used as seed of CG and, to maintain the main characteristics of the path produced by Algorithm 1, some nodes are not affected by the CG because we anchor them to the Algorithm 1 solution. A node is anchored if it is the first or final node of the path, and if it changes the direction of motion of the car. Next, we describe the three terms of the objective function $C(P')$.

The smoothness cost c_c^i is defined as

$$c_s^i = |\Delta p_{i+1} - \Delta p_i|^2, \quad (6)$$

where $\Delta p_i = p_i - p_{i-1}$. The minimization of c_s^i is meant to keep consecutive poses close to one another. However, in doing so, poses may get too close to obstacles, or the steering needed for going from one pose to another may exceed the limits of curvature of the car. To avoid that, we employ the costs c_o^i and c_c^i.

The obstacle cost c_o^i is defined as:

$$c_o^i = \sigma_o(d_{max} - \mathbf{ODGM}[p_i]) \times [\mathbf{ODGM}[p_i] \leq d_{max}] \quad (7)$$

where σ_o is a quadratic penalty function (we use $\sigma_o = (d_{max} - \mathbf{ODGM}[p_i])^2$) and d_{max} is a limit for the value of c_o^i; if $\mathbf{ODGM}[p_i] > d_{max}$, $c_o^i = 0$. As $\mathbf{ODGM}[p_i]$ is the distance from the car at pose p_i to the nearest obstacle, c_o^i increases as the car gets closer to an obstacle up to a maximum equal to ${d_{max}}^3$, in case of a collision.

The curvature cost c_c^i is defined as:

$$c_c^i = \sigma_c\left(\frac{\Delta\phi_i}{|\Delta p_i|} - k_{max}\right) \times \left[\frac{\Delta\phi_i}{|\Delta p_i|} > k_{max}\right] \quad (8)$$

where $\sigma_c = \left(\frac{\Delta\phi_i}{|\Delta p_i|} - k_{max}\right)^2$ is a quadratic penalty function, analogous to the one in the obstacle cost, and $\Delta\phi_i = |atan2(\Delta p_{i+1}.y, \Delta p_{i+1}.x) - atan2(\Delta p_i.y, \Delta p_i.x)|$ is the absolute value of the change in of the tangential angle of P' at p_i. So, $\frac{\Delta\phi_i}{|\Delta p_i|}$ approximates the curvature of P' at p_i. In (8), if the approximate curvature is smaller than the parameter k_{max}, $c_c^i = 0$, otherwise, c_c^i grows unboundedly with $\left(\frac{\Delta\phi_i}{|\Delta p_i|}\right)^3$.

The CG algorithm requires the derivative of $C(P')$ with respect to the x_i and y_i of each p_i of P'. We compute these derivatives numerically.

Our technique for smoothing P' and obtaining P operates only with the x_i and y_i of each p_i. The value r_i of each p_i of P is the same as that computed by the Algorithm 1 for P'. The value θ_i of each p_i of P is defined as $atan2(\Delta p_i.y, \Delta p_i.x)$, for $r_{i-1} = 0$, and $atan2(\Delta p_i.y, \Delta p_i.x) + \pi$, for $r_{i-1} = 1$.

4 EXPERIMENTAL METHODOLOGY

In this section, we describe the methodology used in the experiments conducted to evaluate the performance of the proposed path planner. Firstly, we describe the infrastructure of our self-driving car. Subsequently, we present the parameters of the PPUE implementation examined in the experiments.

Our self-driving car (Figure 1) is based on a Ford Escape Hybrid, which was modified to: allow electronic control of steering, throttle, brakes, gears and several signalization items; provide the car odometry for the its autonomy system; and to supply power for computers and sensors. Its autonomy system follows the typical architecture of self-driving cars – its hardware and software are described by Badue et al. (2020).

The parameters of the PPUE were determined experimentally in an ad hoc manner by means of simulation. We found that $w_1 = 2$, $w_2 = 5$ (see (4)), $\mathbf{ODGM}$ with size of $210\,\text{m} \times 210\,\text{m}$ and with $0.2\,\text{m}$ resolution, $\mathbf{GDM}$ with $210\,\text{m} \times 210\,\text{m}$ and $1\,\text{m}$ of resolution; $\mathbf{NHCM}$ with $100\,\text{m} \times 100\,\text{m} \times 360°$ and 0.2 m resolution for x and y, and 5° for θ, $\mathbf{GSM}$ with size of $210\,\text{m} \times 210\,\text{m} \times 360° \times 2$ and $1\,\text{m}$ resolution for x and y, $10°$ for θ, and 2 directions for r (forward or reverse), $d = 1.41$ m, max-left $= 0.52$ radians, max-right $= 0.52$ radians (Section 3.6), $d_{max} = 1.5$ m, and $k_{max} = 0.17$ m^{-1} (Section 3.8) provided suitable operation of PPUE. We used the Gnu Scientific Library (Galassi et al., 2009) implementation of CG (Section 3.8) in our code.

5 EXPERIMENTAL RESULTS

In this section, we present the results of some experiments we performed to show the performance of PPUE. Initially, three scenarios were considered, all involving entering or exiting a parking lot of the main campus of our university. Figure 5 shows these three experimental simulation scenarios.

In the first scenario (Figure 5(a)), p_1 was positioned in the right lane of the ring road of the our university main campus in clockwise direction, and $p_{|P|}$ was placed in a slot of the parking lot in a top-bottom direction – in this first scenario, the planned path went only forward, from the initial pose in the road, until the final pose in the parking slot. In the second scenario (Figure 5(b)), p_1 and $p_{|P|}$ were positioned in the same poses of the first scenario, except that $p_{|P|}$ was set in the opposite direction (bottom-top) – in this second scenario, the planned path went forward from the initial pose in the lane until the parking lot, and then backward for a couple of meters in order to stop in the parking slot. Finally, in the third scenario (Figure 5(c)), p_1 was placed in another parking slot in top-bottom direction, and $p_{|P|}$ further ahead in the right lane of the ring road in the clockwise direction – in this third scenario, the planned path went backward for a couple of meters, and then forward in order to follow the lane outside the parking lot.

For each one of these three simulation scenarios, we measured the hybrid A* search running time, the whole PPUE running time (hybrid A* plus path smoothing), the number of nodes expanded by the hybrid A* algorithm, and the length of the final smoothed path, P. Table 1 shows these results for an average of five runs of the simulation scenarios.

Table 1: Hybrid A* search time, full PPUE time, number of nodes expanded, and length of the final path for an average of five runs.

Scenario	Search time	Full time	Number of nodes
1	0.42 s	0.64 s	1,248
2	0.61 s	0.76 s	9,450
3	0.47 s	0.51 s	1,170

As shown in Table 1, the hybrid A* search times of the second and third scenarios were larger than that of the first one, because of the penalties involved in the segments of reverse driving present on them. The full running time of the second scenario was the largest of all because of the complexity of the maneuvers required to achieve the goal, which required a larger expansion of nodes during the hybrid A* search.

For all these three simulation scenarios, we measured the time to build the $\mathbf{ODGM}$ and to query it for the distance from the car to the nearest obstacle. $\mathbf{ODGM}$ building time was 0.01 s and $\mathbf{ODGM}$ querying time was 737 ns, for an average of five runs of the simulation scenarios. These running times are well within the 0.05 s time budget allowed by proper operation of the autonomous software system of our self-driving car.

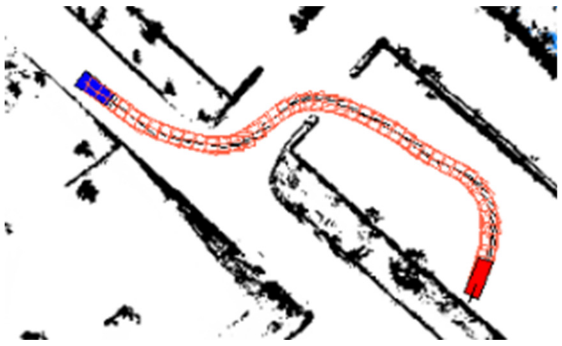
(a)

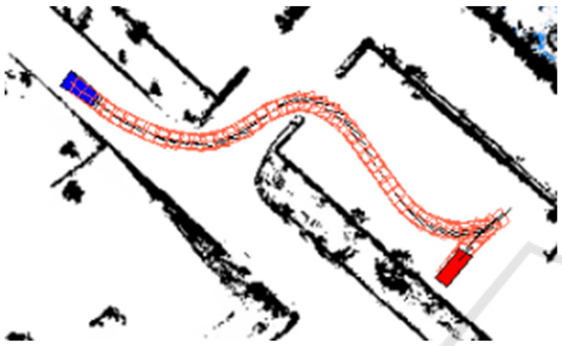
(b)

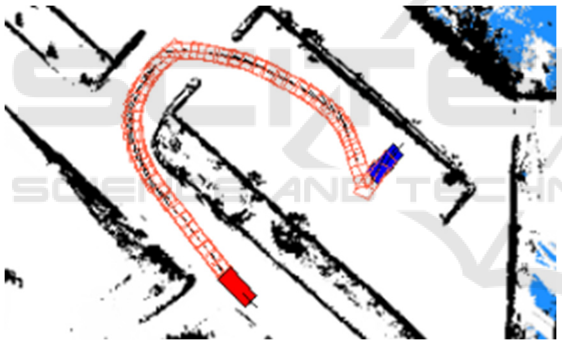
(c)

Figure 5: Experimental simulation scenarios. The blue filled rectangles represent the Initial Pose, p_1, the red filled rectangles the Final Pose, $\mathrm{p}_{|\mathrm{P}|}$, and the sequence of red unfilled rectangles the smoothed paths from p_1 to $\mathrm{p}_{|\mathrm{P}|}$.

In two additional simulation scenarios, we measured the number of nodes expanded by the hybrid A* search using two different $h(.)$ functions: (i) simply the Euclidean distance between p_1 and $p_{|P|}$, and (ii) the $h(.)$ function presented in (3). Figure 6 shows the search tree for each one of these two heuristics.

Using the Euclidean distance between p_1 and $p_{|P|}$ as $h(.)$, hybrid A* expands 8,028 nodes (Figure 6(a)), while using $h(n') = \max\left(\mathbf{GDM}[n'.p], \mathbf{NHCM}\left[p_{|P|} - n'.p\right]\right)$, 6,346 nodes (Figure 6(b)) – the use of **GDM** and **NHCM** reduces the number of expanded nodes significantly. Also, it is easily visible in Figure 6(a) that, when not using **GDM**, hybrid A* searches for solutions in regions of the map that do not offer a path to the goal due to obstacles (see also Figure 4(c)) and, thanks to **NHCM**, the path approaches the goal more smoothly in Figure 6(b).

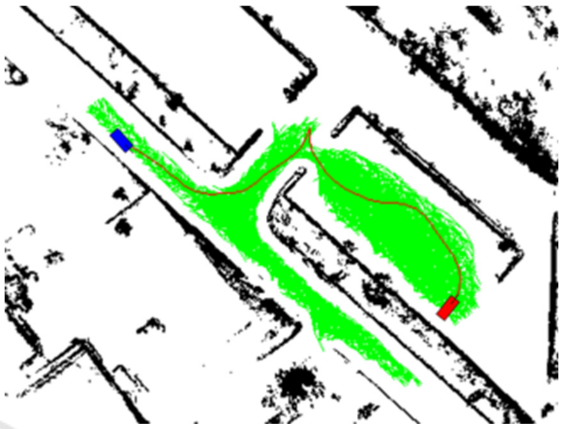
(a)

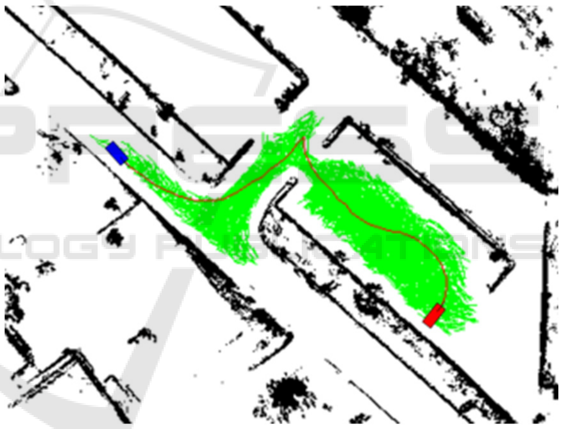
(b)

Figure 6: Search trees for two different $\mathrm{h}(.)$ functions: (a) Euclidean distance; (b) $\mathrm{h}(\mathrm{n}') = \max\left(\mathrm{GDM}[\mathrm{n}'.\mathrm{p}], \mathrm{NHCM}\left[\mathrm{p}_{|\mathrm{P}|} - \mathrm{n}'.\mathrm{p}\right]\right)$. Blue filled rectangles represent the Initial Pose, p_1, red filled rectangles the Final Pose, $\mathrm{p}_{|\mathrm{P}|}$, green curves expanded nodes, and red curves smoothed paths from p_1 to $\mathrm{p}_{|\mathrm{P}|}$.

Finally, we evaluated the performance of the proposed Path Planner for Unstructured Environments in real world scenarios using our self-driving car. A video that shows these experiments is available at http://tiny.cc/iara-ppue. In the video, the first real world scenario is similar to the first simulation scenario (Figure 5(a)), in which the car travels forward from the initial pose in the road to the final pose in a slot of the parking lot. The second scenario in the video shows the car traveling forward from a slot in the parking lot to the road. Finally, in the third scenario, the car is already inside the parking lot and it travels backward until the parking slot. As the video shows, our self-driving car operates appropriately in the real world with PPUE.

6 CONCLUSIONS

We presented a path planner for unstructured urban environments (PPUE) for our or any other self-driving car. PPUE computes smooth and safe paths that obey the kinematic constraints of the vehicle in an amount of time suitable for real world operation. Compared with related works, PPUE differs in its car's collision model and in its use of an obstacle distance map instead of an occupancy grid map – these improvements allow for faster path computation.

As directions for future works, we plan to extend PPUE for allowing its use with semi-trailer trucks.

ACKNOWLEDGEMENTS

This study was financed in part by Coordenação de Aperfeiçoamento de Pessoal de Nível Superior – Brasil (CAPES) – Finance Code 001; Conselho Nacional de Desenvolvimento Científico e Tecnológico - Brasil (CNPq) - grants 310330/2020-3, 133864/2019-7 and 311654/2019-3; and Fundação de Amparo à Pesquisa do Espírito Santo - Brasil (FAPES) – grants 75537958 and 84412844.

REFERENCES

Badue, C., Guidolini, R., Carneiro, R. V., Azevedo, P., Cardoso, V. B., Forechi, A., Jesus, L. F. R., Berriel, R. F., Paixão, T. M., Mutz, F., Oliveira-Santos, T., and De Souza, A. F. (2020). Self-driving cars: A survey. *Expert Systems with Applications*, 113816.

Cardoso, V., Oliveira, J., Teixeira, T., Badue, C., Mutz, F., Oliveira-Santos, T., Veronese, L., and De Souza, A. F. (2017, May). A model-predictive motion planner for the IARA autonomous car. In *2017 IEEE International Conference on Robotics and Automation (ICRA)* (pp. 225-230). IEEE.

Chu, K., Kim, J., Jo, K., and Sunwoo, M. (2015). Real-time path planning of autonomous vehicles for unstructured road navigation. *International Journal of Automotive Technology*, *16*(4), 653-668.

Dolgov, D., Thrun, S., Montemerlo, M., and Diebel, J. (2010). Path planning for autonomous vehicles in unknown semi-structured environments. *The international journal of robotics research*, *29*(5), 485-501.

Elizondo-Leal, J. C., Parra-González, E. F., and Ramírez-Torres, J. G. (2013). The exact Euclidean distance transform: a new algorithm for universal path planning. *International Journal of Advanced Robotic Systems*, *10*(6), 266.

Galassi, M., Davies, J., Theiler, J., Gough, B., Jungman, G., Alken, P., Booth, M., and Rossi, F. (2009). GNU scientific library Reference Manual (3rd Ed). Network Theory Limited.

Ghosh, D., Nandakumar, G., Narayanan, K., Honkote, V., and Sharma, S. (2019, May). Kinematic constraints based Bi-directional RRT (KB-RRT) with parameterized trajectories for robot path planning in cluttered environment. In *2019 International Conference on Robotics and Automation (ICRA)* (pp. 8627-8633). IEEE.

Guidolini, R., Badue, C., Berger, M., de Paula Veronese, L., and De Souza, A. F. (2016, November). A simple yet effective obstacle avoider for the IARA autonomous car. In *2016 IEEE 19th International Conference on Intelligent Transportation Systems (ITSC)* (pp. 1914-1919). IEEE.

Guidolini, R., De Souza, A. F., Mutz, F., and Badue, C. (2017, May). Neural-based model predictive control for tackling steering delays of autonomous cars. In *2017 International Joint Conference on Neural Networks (IJCNN)* (pp. 4324-4331). IEEE.

Kicki, P., Gawron, T., and Skrzypczyński, P. (2020). A Self-Supervised Learning Approach to Rapid Path Planning for Car-Like Vehicles Maneuvering in Urban Environment. *arXiv preprint arXiv:2003.00946*.

Montemerlo, M., Becker, J., Bhat, S., Dahlkamp, H., Dolgov, D., Ettinger, S., Haehnel, D., Hilden, T., Hoffmann, G., Huhnke, B., Johnston, D., Klumpp, S., Langer, D., Levandowski, A., Levinson, J., Marcil, J., Orenstein, D., Paefgen, J., Penny, I., Petrovskaya, A., Pflueger, M., Stanek, G., Stavens, D., Vogt, A., and Thrun, S. (2008). Junior: The stanford entry in the urban challenge. *Journal of field Robotics*, *25*(9), 569-597.

Moraes, G., Mozart, A., Azevedo, P., Piumbini, M., Cardoso, V. B., Oliveira-Santos, T., De Souza, A. F., and Badue, C. (2020, July). Image-Based Real-Time Path Generation Using Deep Neural Networks. In *2020 International Joint Conference on Neural Networks (IJCNN)* (pp. 1-8). IEEE.

Mutz, F., Veronese, L. P., Oliveira-Santos, T., de Aguiar, E., Cheein, F. A. A., and De Souza, A. F. (2016). Large-scale mapping in complex field scenarios using an autonomous car. *Expert Systems with Applications*, *46*, 439-462.

Possatti, L. C., Guidolini, R., Cardoso, V. B., Berriel, R. F., Paixão, T. M., Badue, C., De Souza, A. F., and Oliveira-Santos, T. (2019, July). Traffic light recognition using deep learning and prior maps for autonomous cars. In *2019 International Joint Conference on Neural Networks (IJCNN)* (pp. 1-8). IEEE.

Reeds, J., and Shepp, L. (1990). Optimal paths for a car that goes both forwards and backwards. *Pacific journal of mathematics*, *145*(2), 367-393.

Sarcinelli, R., Guidolini, R., Cardoso, V. B., Paixão, T. M., Berriel, R. F., Azevedo, P., De Souza, A. F., Badue, C., and Oliveira-Santos, T. (2019). Handling pedestrians in self-driving cars using image tracking and alternative path generation with Frenét frames. *Computers & Graphics*, *84*, 173-184.

Thrun, S., Burgard, W., and Fox, D. (2006). Probalistic robotics. *Kybernetes*.

Torres, L. T., Paixão, T. M., Berriel, R. F., De Souza, A. F., Badue, C., Sebe, N., and Oliveira-Santos, T. (2019, July). Effortless deep training for traffic sign detection using templates and arbitrary natural images. In *2019 International Joint Conference on Neural Networks (IJCNN)* (pp. 1-7). IEEE.

Urmson, C., Anhalt, J., Bagnell, D., Baker, C., Bittner, R., Clark, M. N., Dolan, J., Duggins, D., Galatali, T., Geyer, C., Gittleman, M., Harbaugh, S., Hebert, M., M. Howard, T., Kolski, S., Kelly, A., Likhachev, M., McNaughton, M., Miller, N., Peterson, K., Pilnick, B., Rajkumar, R., Rybski, P., Salesky, B., Seo, Y.-W., Singh, S., Snider, J., Stentz, A., "Red" Whittaker, W., Wolkowicki, Z., Ziglar, J., Bae, H., Brown, T., Demitrish, D., Litkouhi, B., Nickolaou, J., Sadekar, V., Zhang, W., Struble, J., Taylor, M., Darms, M. and Ferguson, D. (2008). Autonomous driving in urban environments: Boss and the urban challenge. *Journal of Field Robotics*, *25*(8), 425-466.

Veronese, L. D. P., Guivant, J., Cheein, F. A. A., Oliveira-Santos, T., Mutz, F., de Aguiar, E., Badue, C., and De Souza, A. F. (2016, November). A light-weight yet accurate localization system for autonomous cars in large-scale and complex environments. In *2016 IEEE 19th International Conference on Intelligent Transportation Systems (ITSC)* (pp. 520-525). IEEE.

Wang, Y. (2019, May). Improved A-search guided tree construction for kinodynamic planning. In *2019 International Conference on Robotics and Automation (ICRA)* (pp. 5530-5536). IEEE.

Yoon, S., Yoon, S. E., Lee, U., & Shim, D. H. (2015). Recursive path planning using reduced states for car-like vehicles on grid maps. *IEEE Transactions on Intelligent Transportation Systems*, *16*(5), 2797-2813.